Interaction of Ionic Biomolecular Building Blocks with Nonpolar Solvents: Acidity of the Imidazole Cation (Im^+) Probed by IR Spectra of Im^+-L_n Complexes ($L = Ar, N_2$; $n \leq 3$)

Horia-Sorin Andrei, Nicola Solcà, and Otto Dopfer*

Institut für Physikalische Chemie, Universität Würzburg, Am Hubland, D-97074 Würzburg, Germany

Received: December 23, 2004; In Final Form: February 14, 2005

The intermolecular interaction between the imidazole cation ($Im^+ = C_3N_2H_4^+$) and nonpolar ligands is characterized in the ground electronic state by infrared photodissociation (IRPD) spectroscopy of size-selected Im^+-L_n complexes ($L = Ar, N_2$) and quantum chemical calculations performed at the UMP2/6-311G(2df,2pd) and UB3LYP/6-311G(2df,2pd) levels of theory. The complexes are created in an electron impact cluster ion source, which predominantly produces the most stable isomers of a given cluster ion. The analysis of the size-dependent frequency shifts of both the N−H and the C−H stretch vibrations and the photofragmentation branching ratios provides valuable information about the stepwise microsolvation of Im^+ in a nonpolar hydrophobic environment, including the formation of structural isomers, the competition between various intermolecular binding motifs (H-bonding and π-bonding) and their interaction energies, and the acidity of both the CH and NH protons. In line with the calculations, the IRPD spectra show that the most stable Im^+-L dimers feature planar H-bound equilibrium structures with nearly linear H-bonds of L to the acidic NH group of Im^+. Further solvation occurs at the aromatic ring of Im^+ via the formation of intermolecular π-bonds. Comparison with neutral Im−Ar demonstrates the drastic effect of ionization on the topology of the intermolecular potential, in particular in the preferred aromatic substrate−nonpolar recognition motif, which changes from π-bonding to H-bonding.

I. Introduction

Imidazole ($C_3N_2H_4$, henceforth denoted Im) is a planar heterocyclic aromatic molecule (Figure 1) and occurs as an essential constituent in many biomolecular building blocks, such as the DNA bases adenine and guanine, and the histidine residue of proteins.[1] In aqueous biological environments, Im and its charged and protonated analogues are involved in electron transfer in photosynthesis, in many biologically important enzymatic processes, in protein structure determination, and in proton shuttles.[1−4] The important role of aromatic molecules and their cations for biological and chemical recognition as well as organic reaction mechanisms has also been emphasized in recent reviews.[5−8] Fundamental understanding of these phenomena at the molecular level requires the detailed knowledge of the intermolecular potential of $Im^{(+)}$ and ImH^+ interacting with the surrounding environment. The present work reports IR spectra and quantum chemical calculations of Im^+ solvated by a well-defined number of nonpolar ligands ($L = Ar, N_2$) to elucidate the interaction of the radical cation of this basic biomolecular building block with a hydrophobic environment.

The solute molecule Im offers several principal binding sites for solvent molecules. The ligand can interact with the π-electron system of the aromatic ring (π-bond), form H-bonds to the acidic protons of Im (N−H−L or C−H−L), or serve as a proton donor in a H-bond to the basic N atom of Im. The preferred binding motif of the $Im^{(+)}-L$ interaction strongly depends on the charge state of $Im^{(+)}$ and fundamental properties of L, such as its polarity and proton donor and proton acceptor abilities. In contrast to related aromatic complexes, relatively few gas-phase spectroscopic data exist for neutral Im−L complexes. One reason might be that the high excitation energy of the first excited singlet state of Im[9] is rather inconvenient for the application of resonant multiphoton excitation schemes, which are frequently employed for aromatic cluster spectroscopy, because of their cluster size, state, and isomer selectivity.[6,10−12] The rotational millimeter wave spectrum of neutral Im−Ar recorded in a supersonic jet is consistent with a π-bound equilibrium structure, which is characterized by an Ar−ring separation of $R \sim 3.5$ Å, an intermolecular stretch frequency and force constant of $\nu_s = 44$ cm^{-1} and $k_s = 2.88$ N m^{-1}, and a dissociation energy of $D_e \sim 300$ cm^{-1}.[13] Apparently, Im prefers π-bonding to nonpolar ligands in its singlet electronic ground state (S_0, $^1A'$), because in this configuration the dispersion interaction between L and the π-electron system of Im is optimized. No information appears to be available for the corresponding Im−N_2 dimer.[14] The quadrupolar N_2 ligand is known for its ability to form both H-bonds and π-bonds to acidic aromatic molecules (A). For example, complexes of N_2 with aniline (A = An)[15] and 1-naphthol (A = 1-Np)[16] feature π-bound equilibrium structures, whereas that with phenol (A = Ph) prefers H-bonding.[17,18] Two major competing interaction motifs were identified for the biologically relevant Im−H_2O interaction by both quantum chemical calculations and Ar matrix isolation IR spectroscopy:[19] N−H−O-type H-bonding between the acidic NH group of Im (proton donor) and the O atom of H_2O (proton acceptor) and O−H−N-type H-bonding between the acidic OH group of H_2O (proton donor) and the basic N atom of Im (proton acceptor).[19−21] These H-bonds are mainly stabilized by electrostatic and induction forces. C−H−O-type H-bonding of H_2O to the less acidic CH groups of Im and π H-bonding of H_2O protons to the π-electron system of Im are predicted to be less stable than both N−H−O-type contacts.[22]

Experimental and theoretical information about the Im^+ radical cation and its complexes with neutral ligands is rather sparse. Early photoelectron, photoionization, and photofrag-

* To whom correspondence should be addressed. E-mail: dopfer@physchemie.uni-wuerzburg.de. Fax: +49 931 8886378.

10.1021/jp0441487 CCC: $30.25
Published on Web 03/31/2005

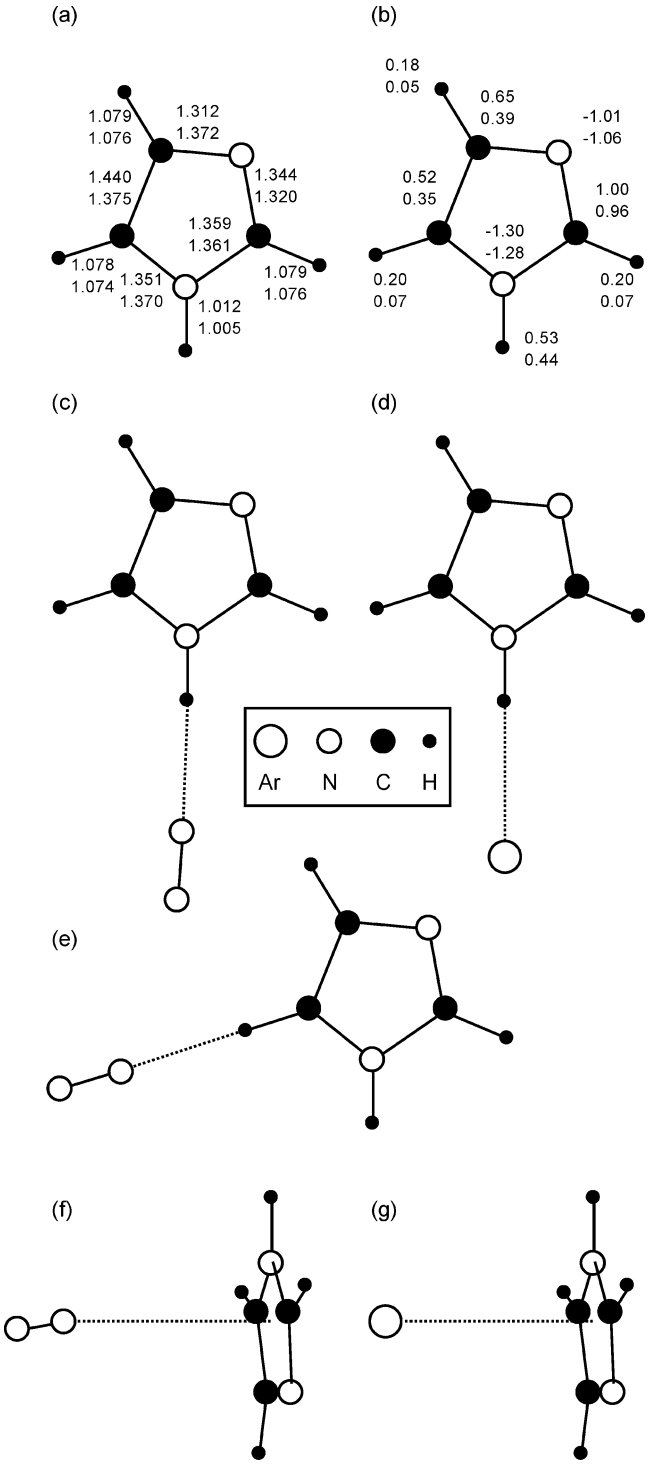

Figure 1. (a) Interatomic distances (Å) in Im^+ (top) and Im (bottom). (b) AIM charges of Im^+ (top) and Im (bottom). (c−g) Minimum structures of $Im^+-N_2(H)$, $Im^+-Ar(H)$, $Im^+-N_2(CH)$, $Im^+-N_2(\pi)$, and $Im^+-Ar(\pi)$. All numbers and geometries with the exception of $Im^+-N_2(CH)$ are evaluated at the UMP2/6-311G(2df,2pd) level.

mentation studies demonstrated that the planar $^2A''$ electronic ground state of Im^+ (D_0) is obtained by removal of one electron from the 3a″ orbital, which is a bonding π-orbital delocalized over the whole aromatic ring.[23−25] Two ring vibrations were identified in the photoelectron spectrum, with frequencies of 970 and 1320 cm^{-1}.[24] No spectroscopic information is available for the N−H and C−H stretch vibrations of Im^+. Recent quantum chemical calculations investigate the structures, vibrational frequencies, IR intensities, and charge distributions of Im and its radical cation, as well as various intermolecular binding motifs of the Im_2^+ homodimer.[26] Neither mass spectrometric nor spectroscopic data seem to be available for any Im^+-L_n complex.[14] Hence, the present spectra of Im^+-Ar and $Im^+-(N_2)_{n\leq 3}$ provide the first spectroscopic information about the structure and stability of Im^+-L_n clusters. As the ionization energy of Im (9.91 eV) is substantially smaller than those of Ar (15.76 eV) and N_2 (15.58 eV),[27] the positive charge in $[Im-Ar]^+$ and $[Im-(N_2)_n]^+$ will be strongly localized on the Im moiety. This large disparity in ionization energies leads to the formation of weakly bound noncovalent Im^+-L_n complexes, which are mainly stabilized by induction and electrostatic forces, whereas contributions from charge transfer to the interaction are negligible.

Ionization of Im is expected to have a large impact on the topology of the intermolecular interaction with both polar and nonpolar ligands, because the excess charge provides additional electrostatic and inductive contributions to the intermolecular attraction.[10,28,29] For example, for acidic aromatic molecules A interacting with rare gas (Rg) atoms or other nonpolar molecules (e.g., CH_4 and N_2), ionization often switches the preferred interaction motif from π-bonding to H-bonding.[29] This $\pi \rightarrow$ H switch was recently observed for the first time for a variety of A−L dimers, including Ph−L (L = Rg, CH_4),[30−33] An−L (L = Ar, N_2),[34,35] 1-Np−Ar,[36] and the Ar complex of indole (In−Ar),[37] and is a general phenomenon for this type of complexes.[29] The ionization-induced $\pi \rightarrow$ H switch in the preferred binding motif can be rationalized by a change in the dominant binding mechanism. In neutral A−L dimers, dispersion forces dominate the attraction and favor π-bonding. On the other hand, induction forces provide the major contribution to the attraction in ionic A^+-L dimers of acidic A and nonpolar L, leading to the preference for H-bonding.[29] In contrast, A−L complexes with nonacidic A and nonpolar L, such as benzene (A = Bz),[12,38−42] feature π-bound equilibrium structures in both the neutral and the cation ground electronic states, because the aromatic CH groups are not sufficiently acidic to make H-bonding more stable than π-bonding. On the basis of these considerations, both Im^+-L dimers investigated in the present work (L = Ar, N_2) are expected to exhibit H-bound global minima, in which L binds to the acidic NH group, and π-bound local minima.

Several aspects motivated the present IR spectroscopic and theoretical study on size-selected Im^+-L_n complexes: (1) These clusters serve as a suitable model for solvation of the highly acidic Im^+ cation in a nonpolar solvent. Of particular interest are the competition between H-bonding and π-bonding and its consequences on the cluster growth. (2) As the ability of the NH group to form H-bonds to a ligand is correlated with its acidity, the IR spectra of H-bound Im^+-L dimers directly probe the acidity of Im^+ and eventually enable a first estimate of the unknown proton affinity of the imidazyl radical. Similarly, the IR spectra of Im^+-L_n provided the first experimental information about the strength of the CH groups in Im^+. (3) The Im^+-Ar/N_2 dimers are also characterized by quantum chemical calculations, because theoretical studies of the interaction potential in these dimers are not available. (4) Comparison of Im−L[13] with Im^+-L and ImH^+-L[43] will reveal the effects of both ionization and protonation of Im on the acidity of the NH protons and the interaction with a nonpolar environment.

II. Experimental Section

IRPD spectra of mass-selected Im^+-L_n complexes (L = Ar and N_2, $n \leq 3$) were recorded in the N−H and C−H stretch ranges using a tandem quadrupole mass spectrometer

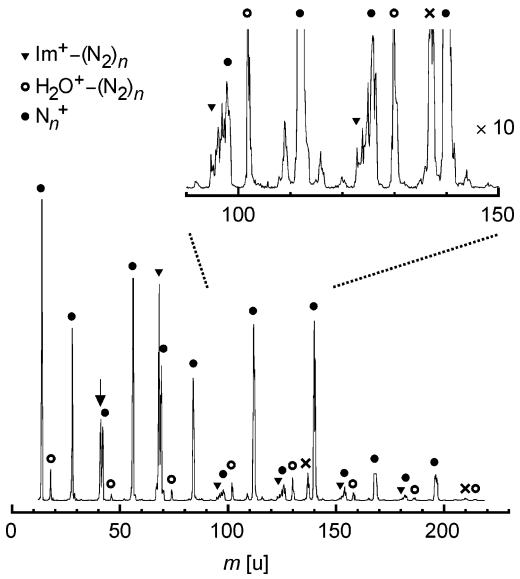

Figure 2. Mass spectrum of the EI ion source obtained for an expansion of Im ($T \approx 370$ K) seeded in 4 bar of N_2. The spectrum is dominated by N_n^+ (filled circles) and $X^+-(N_2)_n$ cluster ions with $X^+ = Im^+$ and ImH^+ (68 and 69 u, triangles), and the impurity H_2O^+ (18 u, open circles). The arrow indicates the dominant fragment peak of Im^+ (41 u, HCN loss). Clusters of the type Im_kH^+ ($k > 1$) are marked by crosses. Part of the spectrum is vertically expanded by a factor of 10 to show weak peaks. The intensity ratios of $Im^+-(N_2)_n$ are on the order of 50: 2.5:2:1 for $n = 0-3$.

(QMS1/2) coupled to an electron impact (EI) ion source and an octopole ion trap.[29,44] Cold ionic clusters were generated in a plasma expansion created by EI of a pulsed supersonic molecular beam. The expanding gas mixture was produced by seeding Im vapor ($T \approx 370$ K) in Ar or N_2 at stagnation pressures of 4−5 bar. Im^+-L_n clusters were produced by EI of Im and subsequent three-body association reactions in the high-pressure region of the expansion.[30,31] This reaction sequence was shown to generate mainly the most stable isomer of a given cluster ion and to a smaller extent less stable isomers.[29−37,45,46] Alternative mechanisms involving the formation of neutral Im−L_n complexes with subsequent EI play only a minor role.[31] Figure 2 shows a mass spectrum of the ion source recorded after optimization for $Im^+-(N_2)_n$ generation. The spectrum is dominated by N_n^+ and $X^+-(N_2)_n$ cluster ions, including $X^+ = Im^+$, ImH^+, and the impurity H_2O^+. The strongest fragment of Im upon EI corresponds to HCN loss, leading to CH_2CNH^+ (41 u), whereas a somewhat weaker fragment channel produces $HCNH^+$ (28 u, CH_2CN loss, blended by the intense N_2^+ peak).[23,47] The intensity ratios of $Im^+-(N_2)_n$ are on the order of 50:2.5:2:1 for $n = 0-3$, confirming the formation of weakly bound noncovalent complexes. The central part of the supersonic plasma expansion was extracted through a skimmer into QMS1, which was tuned to the mass of the desired Im^+-L_n parent cluster. The mass-selected Im^+-L_n beam was then injected into an octopole ion guide, where it interacted with a tunable IR laser pulse. Resonant vibrational excitation of Im^+-L_n induced the evaporation of one or more ligands, according to

$$Im^+-L_n + h\nu \rightarrow Im^+-L_m + (n-m)L \qquad (1)$$

Other photodissociation channels were not observed at the single-photon absorption conditions employed ($I < 200$ kW cm^{-2}).[48,49] The Im^+-L_m fragments generated in the octopole were mass-selected by QMS2 and monitored as a function of the laser frequency (ν) to record the IRPD spectra of Im^+-L_n.

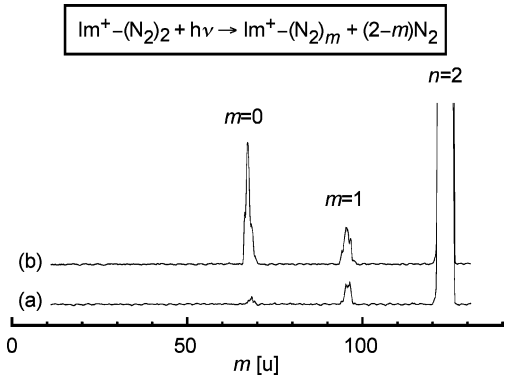

Figure 3. Mass spectra obtained by mass-selecting $Im^+-(N_2)_2$ with QMS1 and scanning QMS2. For spectrum a, the laser was off, and the observed $Im^+-(N_2)_m$ fragment ions ($m = 0$, 1) arise from metastable decay and/or collision-induced dissociation with background gas. For spectrum b, the laser is tuned to the ν_{NH} resonance of $Im^+-(N_2)_2$ at 3313 cm^{-1}, which induces additional fragmentation into both the $m = 0$ and $m = 1$ channels.

For $Im^+-(N_2)_n$ parent complexes with $n > 1$, several fragment channels m were observed. As an example, Figure 3 compares the mass spectra obtained for mass selecting $Im^+-(N_2)_2$ with QMS1 and scanning QMS2 without laser action (a) and with resonant laser excitation (b). Spectrum a displays $m = 0$ and 1 fragment ions arising from metastable decay of hot parent clusters and/or collision-induced dissociation with background gas in the octopole region. The small fraction of metastable decay demonstrates that the $Im^+-(N_2)_2$ complexes reaching the octopole region have relatively little internal energy. Spectrum b reveals additional fragmentation into both the $m = 0$ (83%) and $m = 1$ (17%) fragment channels caused by resonant laser-induced dissociation. To separate laser-induced signals from interfering metastable decay and/or collision-induced dissociation, the ion source was triggered at twice the laser repetition rate and signals from alternating triggers were subtracted. Previous studies on related complexes demonstrated that the IR spectra recorded in the major fragment channels are similar.[31,34,36,37,45,46,50−54] Consequently, IRPD spectra of Im^+-L_n were recorded only in the dominant fragment channel. Tunable IR radiation was generated by a single-mode optical parametric oscillator laser system. Calibration of the laser frequency to an accuracy of better than 1 cm^{-1} was accomplished by comparison to optoacoustic spectra of ammonia recorded simultaneously with the IRPD spectra and by analyzing atmospheric water absorptions along the IR laser path.[55,56]

III. Quantum Chemical Calculations

Ab initio and density functional theory calculations were carried out for Im, Im^+, and several Im^+-L isomers at the UMP2 and UB3LYP levels employing the 6-311G(2df,2pd) basis set to characterize the effects of both ionization and complexation on the properties of imidazole.[57] UB3LYP calculations were shown to reliably describe the properties of H-bonds but fail to properly account for the dispersion interactions, which are significant for π-bonding in A^+-Ar/N_2 dimers.[30] In contrast, the UMP2 calculations yield data with comparable accuracy for both the π-bonds and the H-bonds.[30] All coordinates were relaxed for the search of stationary points, and intermolecular interaction energies were counterpoise corrected for basis set superposition error.[58] The results relevant for the present work are summarized in Figure 1 and Table 1. The table includes structural and energetic attributes of the intermolecular bonds, such as length (R_{HL}, R_{ring-L}), dissociation

TABLE 1: Properties of the Intramolecular N−H and C−H Bonds (R_{NH}, R_{CH}, ν_{NH}, ν_{CH}, I_{NH}, I_{CH}) and the Intermolecular Bonds (R_{HL}, R_{ring-L}, D_e, ν_s) for the Equilibrium Structures of Im, Im^+, and Several Im^+−L Isomers Calculated at the UMP2 and UB3LYP Levels Using the 6-311G(2df,2pd) Basis (Figure 1)

method	molecule	R_{NH}/Å	R_{CH}/Å	$\nu_{NH}{}^a$/cm^{-1}	$\nu_{CH}{}^a$/cm^{-1}	R_{HL}/Å	R_{ring-L}/Å	D_e/cm^{-1}	$\nu_s{}^a$/cm^{-1}
UMP2	Im	1.0045	1.0742	3505 (74)	3120 (3)				
			1.0755		3125 (0)				
			1.0758		3147 (1)				
	Im^+	1.0118	1.0775	3430 (231)	3119 (25)				
			1.0787		3125 (36)				
			1.0793		3136 (16)				
	Im^+−Ar(H)	1.0147	1.0774	3374 (561)	3119 (23)	2.4066		621	66
			1.0786		3125 (36)				
			1.0793		3136 (14)				
	Im^+−N_2(H)	1.0191	1.0774	3301 (818)	3119 (22)	2.0545		1807	106
			1.0786		3126 (33)				
			1.0792		3137 (16)				
	Im^+−Ar(π)	1.0117	1.0774	3433 (227)	3119 (24)		3.42	451	52
			1.0786		3125 (35)				
			1.0793		3136 (16)				
	Im^+−N_2(π)	1.0114	1.0773	3436 (224)	3119 (22)		3.12	1056	75
			1.0786		3126 (33)				
			1.0792		3137 (16)				
UB3LYP	Im	1.0046	1.0749	3513 (50)	3109 (7)				
			1.0767		3112 (0)				
			1.0775		3141 (2)				
	Im^+	1.0131	1.0792	3430 (209)	3109 (21)				
			1.0797		3116 (45)				
			1.0799		3122 (7)				
	Im^+−Ar(H)	1.0166	1.0791	3362 (547)	3110 (21)	2.4708		520	59
			1.0796		3118 (45)				
			1.0797		3124 (3)				
	Im^+−N_2(H)	1.0212	1.0790	3287 (833)	3110 (20)	2.0780		1615	103
			1.0796		3118 (40)				
			1.0796		3125 (4)				
	Im^+−N_2(CH)	1.0128	1.0796	3434 (200)	3087 (157)	2.3874		886	70
			1.0798		3112 (26)				
			1.0815		3120 (8)				
	Im^+−Ar(π)	1.0130	1.0787	3432 (205)	3111 (20)		3.52[b]	172	48
			1.0795		3118 (37)				
			1.0798		3127 (11)				
	Im^+−N_2(π)	1.0128	1.0780	3434 (202)	3113 (19)		3.22[b]	673	70
			1.0793		3118 (30)				
			1.0797		3132 (18)				

[a] Harmonic frequencies are scaled by a factor of 0.9465 (UMP2) and 0.9597 (UB3LYP). IR intensities (I_{NH} and I_{CH}, km mol^{-1}) are listed in parentheses. [b] Distance to the nearest C atom.

energy (D_e), and intermolecular stretch frequency (ν_s), as well as relevant properties of the intramolecular N−H and C−H bonds, namely, length (R_{NH}, R_{CH}), stretch frequency (ν_{NH}, ν_{CH}), and IR intensity (I_{NH}, I_{CH}). Harmonic vibrational frequencies were scaled by a factor of 0.9465 (UMP2) and 0.9597 (UB3LYP) to match the calculated N−H stretch frequencies of Im^+ with the experimental one estimated from the IRPD spectrum of Im^+−Ar (vide infra, ν_{NH} = 3430 cm^{-1}). For the monomers and H-bound dimers, the UMP2 and UB3LYP calculations yield similar energetic, structural, and vibrational data. In contrast, for the π-bound dimers only the UMP2 data are considered, because the UB3LYP data fail to describe dispersion.

Geometry optimization in the ground electronic state of both Im (^{1}A′, S_0) and Im^+ (^{2}A″, D_0) results in planar equilibrium structures with C_s symmetry. The relevant geometrical parameters and the charge distributions evaluated using the atoms-in-molecules (AIM) population analysis are compared in parts a and b of Figure 1, respectively. Ionization of Im removes an electron from the bonding 3a″ molecular orbital, which is delocalized over the aromatic ring.[24] As a consequence, the ring opens slightly up upon ionization, giving rise to Franck−Condon activity in the two symmetric ring stretch modes observed in the He(I) photoelectron spectra.[24] Simultaneously, the N−H and all three C−H bonds become weaker and longer, inducing shifts in the corresponding stretch frequencies of $-\Delta\nu_{CH} < 11$ and $\Delta\nu_{NH} = -75$ cm^{-1}, respectively (UMP2). In addition, ionization also strongly enhances the IR activities of both the ν_{CH} and the ν_{NH} fundamentals, in line with the increased charges on the respective protons derived from the AIM analysis summarized in Figure 1b. The N−H stretch normal mode is essentially localized on the N−H bond, whereas the C−H stretch normal modes are largely delocalized over all three C−H bonds, resulting in similar C−H stretch frequencies. The ν_{NH} and ν_{CH} frequencies calculated for neutral Im at the UMP2 and UB3LYP levels show deviations of less than 26 cm^{-1} from the measured values (ν_{NH} = 3518 cm^{-1}, ν_{CH} = 3160, 3135, and 3135 cm^{-1}),[59] demonstrating that the chosen theoretical levels appropriately describe the monomer properties. Comparison of the AIM population analysis of Im and Im^+ reveals that the additional positive charge is mainly distributed over the two neighboring ring C atoms and the four protons. In general, the AIM analysis yields a charge distribution very different from those of the corresponding Mulliken population analyses obtained in the present work and in ref 26. The Mulliken approach is, however, known to be very sensitive to the theoretical level, whereas the AIM method provides reliable and level-independent charge distributions.[60] Hence, the Mulliken charges are not considered further.

The intermolecular Im^+−L dimer potentials feature planar H-bound global minima with C_s symmetry, denoted Im^+−L(H), with nearly linear H-bonds between L and the acidic NH group of Im^+ as shown in Figure 1c,d. The deviations of the N−H−L bonds from linearity are less than 0.5°. The anisotropy of the

long-range charge−quadrupole and charge−induced dipole interactions aligns the N_2 ligand in such a way that the diatomic axis points toward the positive charge,[28,30,34,36,37,45,50,61−65] resulting in nearly linear H···N−N configurations in $Im^+-N_2(H)$. N_2 has a larger parallel polarizability than Ar (2.38 and 1.64 Å^3) and an additional quadrupole moment (−5.00 C m^2),[66−68] leading to a stronger induction and electrostatic attraction in the N_2-containing complexes. Consequently, the H-bond in $Im^+-N_2(H)$ is stronger than in $Im^+-Ar(H)$, leading to a shorter H−L bond (R_{HL}/Å = 2.08 and 2.47), with a larger stretch frequency (ν_s/cm^{-1} = 103 and 59) and a higher dissociation energy (D_e/cm^{-1} = 1615 and 520). The effects of H-bonding on the intramolecular N−H bond are an elongation (ΔR_{NH}), a reduction in the stretch frequency ($\Delta\nu_{NH}$), and an enhancement in the IR oscillator strength (ΔI_{NH}). Again, the magnitude of these effects is correlated with the H-bond strength: ΔR_{NH}/Å = 0.0035 and 0.0081, $\Delta\nu_{NH}$/cm^{-1} = −68 and −143, and ΔI_{NH} = 162 and 299% for L = Ar and N_2, respectively. These theoretical results demonstrate that IR spectroscopy in the N−H stretch range is a suitable tool to probe the acidity of the NH group in Im^+ and its ability to form H-bonds.

In addition to the H-bound global minima, the Im^+-L potentials possess less stable π-bound local minima, denoted $Im^+-L(\pi)$. As can be seen from the geometries shown in Figure 1f and 1g, the ligands are roughly located above the center of the aromatic ring. Moreover, the N_2 ligand in $Im^+-N_2(\pi)$ is aligned nearly perpendicularly to the aromatic plane and pointing toward the positive charge. Similar to the H-bond in $Im^+-L(H)$, the intermolecular π-bond in $Im^+-N_2(\pi)$ is more stable than in $Im^+-Ar(\pi)$, as demonstrated by the shorter ring−L separation (R_{ring-L}/Å = 3.12 and 3.42), the larger stretch frequency (ν_s/cm^{-1} = 75 and 52), and the higher dissociation energy (D_e/cm^{-1} = 1056 and 451). Intermolecular π-bonding has only modest effects on the properties of both the N−H and the C−H bonds of Im^+, with $|\Delta R_{NH}| < 0.0004$ Å, $|\Delta R_{CH}| < 0.0002$ Å, $\Delta\nu_{NH} \le 6$ cm^{-1}, $\Delta\nu_{CH} \le 1$ cm^{-1}, $\Delta I_{NH} < 5\%$, and $\Delta I_{CH} < 17\%$. As expected, the UB3LYP calculations fail to reliably describe the π-bonds in $Im^+-L(\pi)$.[30] They yield equilibrium structures in which the ligands are largely displaced from the center of the aromatic ring toward the C−C bond. Moreover, the dissociation energies are much lower than those obtained at the UMP2 level.

H-bonding of L to the aromatic CH groups yields further local minima on the Im^+-L potentials, denoted $Im^+-L(CH)$, which have only been optimized for L = N_2 employing the UB3LYP level. One such example for $Im^+-N_2(CH)$ is selected and included in Figure 1e and Table 1. According to the UB3LYP calculations, this particular isomer is the most stable one among the three possible $Im^+-N_2(CH)$ isomers (D_e = 886, 831, and 693 cm^{-1}), in line with the highest positive partial charge on the corresponding CH proton (q_H = 0.20, 0.20, and 0.18 e). In general, the H-bonds to the CH groups are significantly less stable than the H-bond to the NH group. This result is consistent with the larger acidity of the NH group and the larger positive partial charge on the corresponding proton (q_H = 0.53 e). Significantly, the unambiguous spectroscopic signature of the $Im^+-N_2(CH)$ isomers is the noticeable red shift in the frequency (∼−20 cm^{-1}) and the strong enhancement in the IR intensity (by a factor of ∼8) of the stretch vibration of the CH group acting as the proton donor (Table 1). Comparison of the UMP2 and UB3LYP dissociation energies of $Im^+-N_2(H)$, D_e = 1807 and 1615 cm^{-1}, indicates that the UMP2 values are around 12% larger. Scaling the dissociation energies of the $Im^+-N_2(CH)$ isomers with the same factor yields UMP2 estimates of D_e = 992, 931, and 776 cm^{-1}, which are all lower than the corresponding value for $Im^+-N_2(\pi)$, D_e = 1056 cm^{-1}. The large negative partial charge at the nonprotonated N atom of Im^+, q_N = −1.01 e, suggests that this binding site may also be attractive for neutral ligands. However, test calculations for Im^+-N_2 at the UB3LYP level showed that starting geometries with N_2 near this N atom converged always to one of the neighboring $Im^+-N_2(CH)$ local minima. Hence, the significant Pauli repulsion resulting from the lone pair at this N atom prevents this position from being a favorable binding site in Im^+-L dimers. In contrast, H-bonds to the acidic protons of Im^+ are advantageous binding motifs, because of the significant positive partial charges on these protons and the resulting reduced Pauli repulsion, which allows for a closer approach of L.

According to the calculations, the H-bonds to the NH group in Im^+-L_n are more stable than the π-bonds, which in turn are more stable than the H-bonds to the CH groups. As a result, the energetically most favorable Im^+-L_n cluster growth begins with the formation of a H-bound Im^+-L dimer, to which further π-bound ligands are attached.

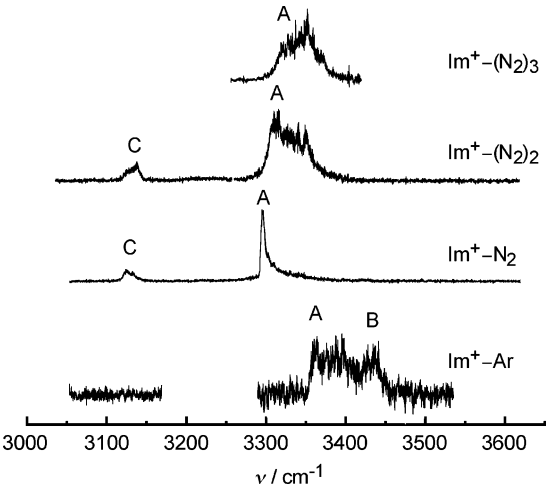

Figure 4. IRPD spectra of Im^+-L_n with L = Ar (n = 1) and L = N_2 (n = 1−3) in the N−H and C−H stretch ranges recorded in the Im^+ fragment channel. The vibrational and isomer assignments of the transitions observed (A−C) are listed in Table 2.

IV. IR Spectra

The IRPD spectra of Im^+-Ar and $Im^+-(N_2)_{n\le3}$ recorded in the C−H and N−H stretch ranges are shown in Figure 4. Table 2 summarizes the band origins and widths of the transitions observed (A−C), along with their vibrational and isomer assignments.

IV.A. Im^+-L Dimers. To assign the vibrational bands observed in the IRPD spectra of the Im^+-L_n clusters, it is instructive to consider the frequencies of the N−H and C−H stretch fundamentals of the isolated Im^+ chromophore. As ν_{NH} and ν_{CH} of bare Im^+ have not been measured yet, they are estimated in the present work using the following two approaches. The first one employs the experimental frequencies of neutral Im (ν_{NH} = 3518 cm^{-1} and ν_{CH} = 3160, 3135, and 3135 cm^{-1})[59] and the ionization-induced shifts predicted by the UB3LYP calculations ($\Delta\nu_{NH}$ = −83 cm^{-1} and $\Delta\nu_{CH}$ = −19, 4, and 0 cm^{-1}), yielding estimated frequencies of ν_{NH} = 3435 cm^{-1} and ν_{CH} = 3141, 3139, and 3135 cm^{-1} for Im^+, respectively. The corresponding UMP2 data ($\Delta\nu_{NH}$ = −75 cm^{-1} and $\Delta\nu_{CH}$ = −11, 0, and −1 cm^{-1}) result in ν_{NH} = 3443 cm^{-1}

TABLE 2: Band Origins and Widths (Fwhm, in Parentheses) of the Transitions Observed in the IRPD Spectra of Im^+-L_n, along with Their Vibrational and Isomer Assignments[a]

ν^b/cm^{-1}	band	vibration	isomer[a]
3361 (52)	A	ν_{NH}	$Im^+-Ar(H)$
3433 (16)	B	ν_{NH}	$Im^+-Ar(\pi)$
3295 (6)	A	ν_{NH}	$Im^+-N_2(H)$
3128 (16)	C	ν_{CH}	$Im^+-N_2(H)$
3313 (54)	A	ν_{NH}	$Im^+-(N_2)_2(H/\pi)$
3132 (20)	C	ν_{CH}	$Im^+-(N_2)_2(H/\pi)$
3323 (60)	A	ν_{NH}	$Im^+-(N_2)_3(H/2\pi)$

[a] (xH/$y\pi$) denotes an isomer with x H-bound and y π-bound ligands ($x + y = n$). [b] For the strongly asymmetric ν_{NH} band of the H-bound isomers (band A), the given position corresponds to the maximum of the P branch head which occurs close to the band origin. For the symmetric bands B and C, the band centers are listed.

and ν_{CH} = 3149, 3135, and 3134 cm^{-1}. The second approach for estimating ν_{NH} of Im^+ employs the measured frequency of the related heterocyclic In^+ cation (ν_{NH} = 3454 cm^{-1})[69] and the ratio of the harmonic frequencies of In^+ and Im^+ (ω_{NH} = 3602 and 3574 cm^{-1}) evaluated at the UB3LYP/6-31G* level.[37] This route yields ν_{NH} = 3427 cm^{-1} for Im^+, in good agreement with the values estimated from the first approach, ν_{NH} = 3435 and 3443 cm^{-1}.

The IRPD spectrum of Im−Ar in Figure 4 displays a rather broad but structured absorption in the N−H stretch range. Two transitions are identified and assigned to the ν_{NH} fundamentals of the H-bound (A) and π-bound (B) isomers of Im^+-Ar. These assignments are based on the band positions, relative IR intensities, and band profiles, as well as the comparison with the quantum chemical calculations. Band B is centered at 3433 cm^{-1} and occurs close to the ν_{NH} frequency predicted above for bare Im^+. The modest estimated complexation-induced shift ($\leq$10 cm^{-1}) and the symmetric band profile are consistent with an assignment to $Im^+-Ar(\pi)$,[30] because intermolecular π-bonding has essentially no influence on the properties of the N−H bond, and vice versa N−H stretch excitation does not affect the properties of the π-bond. The calculations predict a blue shift of $\Delta\nu_{NH}$ = 3 cm^{-1} upon π-bonding with Ar (UMP2), yielding 3430 cm^{-1} as the best experimental estimate for ν_{NH} of bare Im^+. This value has been used for determining the scaling factors employed in section III and Table 1 and will be used throughout this paper for the evaluation of experimental complexation-induced frequency shifts, $\Delta\nu_{NH}$. There are actually other binding sites rather than π-bonding, which also have little impact on the N−H bond, such as the H-bonds to the CH groups. The calculations described in section III, however, suggest that these H-bonds are less stable than the π-bond. This conclusion is further supported by theoretical and spectroscopic data obtained for BzH^+-Ar,[50,70] Bz^+-Ar,[39,41,42,71] and PhH^+-Ar,[72,73] which also demonstrated that the intermolecular CH−Ar bonds in $A(H)^+-Ar$ dimers are less stable than the corresponding π-bonds. The width and shape of band B ($\sim$16 cm^{-1}) could be reproduced by band contour simulations, using an effective rotational temperature of around 150 K and the following realistic approximations. The transition dipole lies along the N−H axis, and the rotational constants (A = 0.160282 cm^{-1}, B = 0.048490 cm^{-1}, C = 0.047647 cm^{-1}) are taken from the UMP2 calculations for $Im^+-Ar(\pi)$ and are assumed to be the same in both vibrational states.

In addition to the ν_{NH} band of the π-bound isomer (B), the Im^+-Ar spectrum reveals a blue shaded band displaying a sharp P branch head near 3361 cm^{-1} (A) and a rather broad R branch around 3400 cm^{-1}. This transition is attributed to ν_{NH} of the H-bound Im^+-Ar isomer shown in Figure 1d. The blue shaded band contour is characteristic for the excitation of a proton donor stretch vibration, because the intermolecular H-bond becomes stronger and shorter in the excited vibrational state, resulting in larger rotational constants.[28,30,46,53,63] The vibrational band origin of such transitions occurs close to the maximum of the P branch. Hence, the latter is taken as an approximate value for the band origin in the present work. The derived red shift upon complexation amounts to $\Delta\nu_{NH}$ = −69 cm^{-1} and agrees well with the value of −68 cm^{-1} calculated at the UB3LYP level. The UMP2 value of $\Delta\nu_{NH}$ = −56 cm^{-1} somewhat underestimates the experimental shift, similar to previous calculations for the O−H stretch fundamental of the related $Ph^+-Ar(H)$ dimer conducted at the same level ($\Delta\omega_{OH}^{calcd}$ = −56 cm^{-1}, $\Delta\nu_{OH}^{exptl}$ = −70 cm^{-1}).[33]

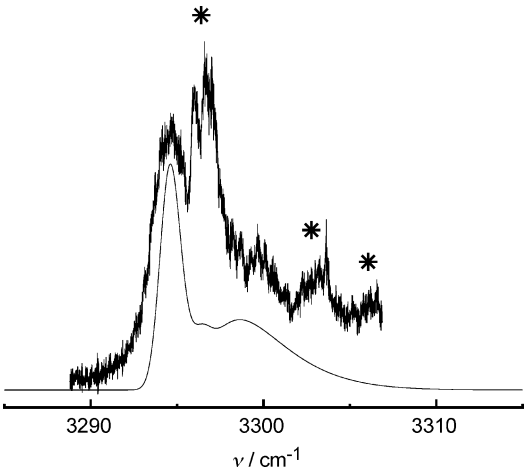

Figure 5. Experimental and simulated IR spectrum of the ν_{NH} band of $Im^+-N_2(H)$. The additional signal in the blue wing of the experimental transition (indicated by asterisks) arises from sequence hot bands, which are not included in the simulation.

In contrast to the N−H stretch range, the Im^+-Ar spectrum reveals no detectable absorption in the C−H stretch range between 3050 and 3170 cm^{-1}. However, as the ν_{CH} fundamentals of both $Im^+-Ar(H)$ and $Im^+-Ar(\pi)$ are predicted to be roughly 1 order of magnitude less intense than ν_{NH}, they cannot be observed at the signal-to-noise levels achieved. One of the reasons for the relatively low signal levels in the Im^+-Ar spectrum results from the large background of metastable decay of the $[N_2-Ar_2]^+$ complex, which has the same mass as Im^+-Ar (m = 108 u) and was produced in significant abundance from the remaining N_2 impurities in the gas inlet system. Hence, the laser-induced dissociation process, $Im^+-Ar \rightarrow Im^+ + Ar$, interfered with the metastable decay process, $[N_2-Ar_2]^+ \rightarrow [N_2-Ar]^+ + Ar$, because both the parent and the daughter ion masses are the same for the two processes.

The Im^+-N_2 spectrum displays a single blue shaded band in the N−H stretch range at around 3295 cm^{-1} (A), which can readily be assigned to ν_{NH} of the H-bound isomer shown in Figure 1c. The observed red shift of $\Delta\nu_{NH}$ = −135 cm^{-1} is compatible with the calculated value of −143 cm^{-1} (UB3LYP). Again, the shift obtained at the UMP2 level, $\Delta\nu_{NH}$ = −129 cm^{-1}, slightly underestimates the experimental one. Figure 5 compares a slow scan of the experimental IR spectrum in the vicinity of the ν_{NH} band with a simulation of the corresponding fundamental transition, using an effective rotational temperature of T = 100 K, a convolution width of 0.3 cm^{-1}, and a band origin of ν_0 = 3296.2 cm^{-1}. Furthermore, the ground-state rotational constants are taken from the UMP2 calculations (A = 0.337307 cm^{-1}, B = 0.032662 cm^{-1}, and C = 0.029779

cm^{-1}), and the upper-state constants are obtained by assuming a contraction of the intermolecular bond of $\Delta R = -0.05$ Å upon ν_{NH} excitation ($A = 0.337318$ cm^{-1}, $B = 0.033268$ cm^{-1}, and $C = 0.030282$ cm^{-1}). A contraction of this magnitude is typical for excitation of proton donor stretch vibrations in proton-bound dimers with this type of interaction energy.[46,53,74−76] The transition dipole is assumed to lie along the N−H bond. Comparison of the experimental and simulated ν_{NH} spectra reveals additional signal in the blue wing of the measured transition (indicated by asterisks in Figure 5), which cannot be reproduced by simulations even under significant variations of both T and ΔR within the physically meaningful parameter space. This additional signal is attributed to sequence transitions of the type $\nu_{NH} + \nu_x \leftarrow \nu_x$, where ν_x are intermolecular vibrations.[28,30] Such transitions were previously observed in related H-bound dimers.[28,30,76] They occur at higher frequency than the ν_{NH} fundamental, because the frequencies of the intermolecular stretch and bend modes increase upon ν_{NH} excitation due to the stronger and more rigid intermolecular bond.[28]

Significantly, no absorption is detected in the Im^+-N_2 spectrum in Figure 4 near 3430 cm^{-1}, implying that the abundances of the $Im-N_2(\pi)$ and $Im-N_2(CH)$ isomers are below the detection limit. In addition to ν_{NH} of $Im^+-N_2(H)$, the Im^+-N_2 spectrum features a band near 3128 cm^{-1} (C), which is attributed to the three overlapping C−H stretch fundamentals, ν_{CH}, of the $Im^+-N_2(H)$ isomer. On the basis of the arguments detailed above, the three ν_{CH} vibrations of bare Im^+ are expected to occur between 3135 and 3141 cm^{-1} (UB3LYP) or between 3134 and 3149 cm^{-1} (UMP2), in good agreement with the observed band. H-bonding at the NH group induces essentially no frequency shifts for ν_{CH} (Table 1), implying that the 3128 cm^{-1} band in the Im^+-N_2 spectrum provides a very good approximation to the bare Im^+ transitions (messenger technique).[41,42] In addition, the ratio of the integrated intensities of the ν_{NH} and ν_{CH} bands (6.5) is consistent with the ratio predicted for $Im^+-N_2(H)$ (∼13, UB3LYP), taking into account that experimental intensity ratios of widely separated bands are only accurate to within a factor of ∼2. The Im^+-N_2 spectrum lacks strong absorptions in the spectral range of the intense ν_{CH} vibrations of the $Im^+-N_2(CH)$ dimers (3050−3100 cm^{-1}), confirming the absence of significant concentrations of these isomers in the molecular beam.

The ratios of the integrated ν_{NH} band intensities observed in the IRPD spectra of Im^+-L can be used to estimate the relative abundances of the H-bound and π-bound isomers in the plasma expansion, using the calculated ν_{NH} IR oscillator strengths given in Table 1. For Im^+-Ar, this procedure results in an abundance ratio of $N_H:N_\pi \approx 1.2$, on the basis of the experimental ν_{NH} intensity ratio of ∼3 and the theoretical ratio of $I_H:I_\pi \approx 2.5$. For Im^+-N_2, a lower limit for $N_H:N_\pi > 10$ can be estimated from the achieved signal-to-noise ratio (∼50) and $I_H:I_\pi \approx 4$. The larger abundance of the $Im^+-L(H)$ isomers suggests that they are more stable than the $Im^+-L(\pi)$ dimers, because the EI source produces predominantly the most stable isomer of a given complex.[31,44] Moreover, the energy difference between both isomers appears to be significantly larger for Im^+-N_2 than for Im^+-Ar, resulting in a much less efficient production of the π-bound isomer for the N_2-containing complex. This observation is in line with the quantum chemical results (Table 1).

IV.B. Larger $Im^+-(N_2)_n$ Complexes. Similar to Im^+-N_2, the IRPD spectrum of the $Im^+-(N_2)_2$ trimer in Figure 4 reveals two bands, A and C, at 3313 and 3132 cm^{-1}, which display only small incremental blue shifts of $\Delta\nu_{NH} = 18$ cm^{-1} and $\Delta\nu_{CH} = 4$ cm^{-1} from the corresponding dimer transitions. Consequently, these bands are assigned to ν_{NH} and ν_{CH} fundamentals of an $Im^+-(N_2)_2$ isomer, which is obtained by adding a π-bound ligand to $Im^+-N_2(H)$, denoted $Im^+-(N_2)_2(H/\pi)$. The ν_{NH} band is again shaded to the blue, but the shading is less prominent as compared to that of the dimer, leading to a larger width of the band and a less pronounced P branch head. The calculations for the $Im^+-N_2(\pi)$ dimer show that a π-bound ligand slightly strengthens the N−H bond ($\Delta R_{NH} = -0.0004$ Å, $\Delta\nu_{NH} = 6$ cm^{-1}). As a result of this N−H bond contraction induced by the second ligand in $Im^+-(N_2)_2(H/\pi)$, the NH group becomes less acidic and the strength of the H-bond to the first N_2 ligand decreases. The large width of band A may also indicate the presence of a less stable isomer, featuring two H-bound ligands interacting with the NH group of Im^+, denoted $In^+-(N_2)_2(2H)$. Such isomers were previously invoked to explain the large incremental blue shift of $\Delta\nu_{NH} = 25$ cm^{-1} observed in the related $In^+-(N_2)_2$ cluster upon complexation with the second ligand.[37] Hence, part of the signal in the blue wing of band A may be attributed to $Im^+-(N_2)_2(2H)$ isomers. Significant contributions of $Im^+-(N_2)_2$ isomers, in which the second ligand forms a H-bond to one of the CH groups, to the observed $Im^+-(N_2)_2$ spectrum can be excluded from the absence of intense absorptions in the spectral range expected for ν_{CH} proton donor stretch vibrations (3050−3100 cm^{-1}). Similar to $Im^+-(N_2)_2$, the $Im^+-(N_2)_3$ spectrum displays a broad and blue shaded band (A) in the N−H stretch range, and the incremental blue shift of $\Delta\nu_{NH} = 10$ cm^{-1} suggests an assignment to an isomer with one H-bound and two π-bound ligands, $Im^+-(N_2)_2(H/2\pi)$. The ν_{NH} frequencies of the most stable isomers of all Im^+-L_n clusters investigated are plotted in Figure 6 as a function of the cluster size n.

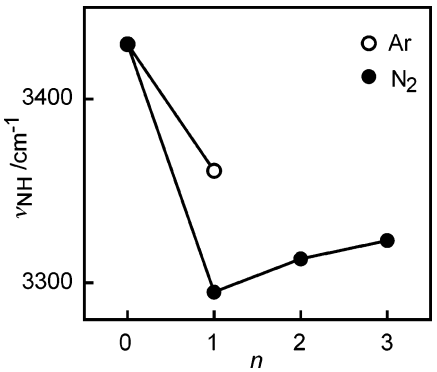

Figure 6. Experimental ν_{NH} frequencies of the most stable Im^+-L_n isomers (L = Ar, N_2) as a function of the cluster size n (Table 2). The calculated frequency is used for bare Im^+ ($n = 0$).

The photofragmentation branching ratios measured for resonant ν_{NH} excitation of the $H/(n-1)\pi$ isomers of $Im^+-(N_2)_n$ provide useful information about the ligand binding energies. In agreement with previous studies on related systems,[31,34,36,37,42,44−46,50,53,72] the range of photoinduced fragment channels (m) for a given parent cluster size (n) is narrow, and at most two major fragment channels are observed. This information can be used to roughly estimate ligand binding energies within the framework of a simple model, which assumes that the absorbed photon energy (ν_{NH}) is available for subsequent ligand evaporation.[31] For this purpose, the ligands are classified as H-bound and π-bound, with dissociation energies of $D_0(H) > D_0(\pi)$. Moreover, all π-bound ligands are assumed to have the same binding energy. The measured branching ratios are $m = 0$ (100%) for $n = 1$, $m = 0$ (83%) and $m = 1$ (17%) for $n = 2$, and $m = 0$ (57%) and $m = 1$

(43%) for $n = 3$. These data suggest that the photon energy of $\nu_{NH} \sim 3300$ cm^{-1} is on the order of the sum of the binding energies of all three ligands in the $Im^+-(N_2)_3(H/2\pi)$ tetramer, leading to the rough estimate of $2D_0(\pi) + D_0(H) \sim 3300$ cm^{-1}. This experimental result is compatible with the quantum chemical well depths of $D_e(\pi) = 1056$ cm^{-1} and $D_e(H) = 1807$ cm^{-1} for the Im^+-N_2 dimer (Table 1).

V. Further Discussion

Both the IRPD spectra and the quantum chemical calculations suggest that the H-bond of Ar to Im^+ is more stable than the π-bond. Recent determinations of accurate binding energies (D_0) of related $A^+-Ar(\pi)$ dimers, such as Bz^+-Ar (512 ± 3 cm^{-1}),[77] *p*-difluorobenzene^+-Ar (572 ± 6 cm^{-1}),[78] In^+-Ar (537 ± 10 cm^{-1}),[79] and Ph^+-Ar (535 ± 3 cm^{-1}),[80] suggest that the strength of the π-bond of Ar to an aromatic cation A^+ is apparently rather insensitive to the detailed structure of A^+. Hence, $D_0(\pi)$ of Im^+-Ar may be estimated as $\sim 550 \pm 100$ cm^{-1}, which is somewhat larger than $D_e = 451$ cm^{-1} obtained at the UMP2 level (Table 1). Assuming that this level underestimates the strength of the π-bond and H-bonds with similar magnitude, the predicted well depth of $D_e(H) = 621$ cm^{-1} results in $D_0(H) \approx 750$ cm^{-1}. The $\Delta\nu_{NH}$ shifts correspond directly to the changes in the intermolecular binding energies upon ν_{NH} excitation. The -69 cm^{-1} shift for $Im^+-Ar(H)$ implies that the H-bond interaction increases by about 10% in the $\upsilon_{NH} = 1$ state. In contrast, the $+3$ cm^{-1} blue shift predicted for $Im^+-Ar(\pi)$ suggests that ν_{NH} excitation only slightly destabilizes the intermolecular π-bond.

The millimeter wave spectrum of neutral Im−Ar has been interpreted with a π-bound global minimum structure.[13] No experimental evidence for the H-bound isomer has been reported so far. The π-bound isomer optimizes the dispersion forces between Ar and the π-electron system of the aromatic ring, which dominate the attractive part of the intermolecular potential in S_0. Ionization of $Im-Ar(\pi)$ enhances the attraction by charge−induced dipole forces, which lead to a contraction of the intermolecular bond. This trend is also evident from the comparison of the potential parameters derived from the millimeter wave spectrum of Im−Ar ($D_e \sim 300$ cm^{-1}, $\nu_s = 44$ cm^{-1}, $R_{ring-Ar} = 3.481$ Å) with the corresponding UMP2 values for Im^+-Ar in Table 1 ($D_e = 451$ cm^{-1}, $\nu_s = 52$ cm^{-1}, $R_{ring-Ar} \sim 3.42$ Å). A similar contraction of $\Delta R_{ring-Ar} = -0.07$ Å upon ionization has also been derived from the analysis of rotationally resolved spectra of $Bz^{(+)}-Ar(\pi)$.[71]

Significantly, the IRPD spectrum and the quantum chemical calculations of Im^+-Ar clearly demonstrate that the H-bond is the preferred intermolecular recognition site in D_0, because of the additional induction forces between the Im^+ charge distribution and the polarizability of Ar. In particular, the large positive partial charge on the acidic NH proton causes the substantial additional stabilization of the H-bond on ionization. The apparent ionization-induced switch in the preferred recognition motif from π-bonding to H-bonding has recently been demonstrated for several $A^{(+)}-Ar$ and $A^{(+)}-CH_4$ dimers involving aromatic molecules $A^{(+)}$ with acidic functional YH_k groups (Y = O, N) and appears to be a general phenomenon.[29] The molecules investigated so far are A = (para-halogenated) Ph,[30−33] An,[35] In,[37] 1-Np,[36] and Im. H-bonds to Ar are also the most stable binding pattern for protonated aromatic molecules (AH^+) featuring acidic functional groups, such as PhH^+, 1-NpH^+, and ImH^+.[36,43,65,72,73] Significantly, Ar and CH_4 prefer intermolecular π-bonds over H-bonds to $A(H)^+$ without acidic substituents, such as $Bz(H)^+$.[42,50,70] Both the aromatic and aliphatic C−H bonds in $A(H)^+$ are only little acidic,[50] so that dispersion forces favoring π-bonds override the induction forces favoring H-bonds.

Similar to $Ph(H)^+-N_2$,[30,31,65,72] An^+-N_2,[34] In^+-N_2,[37] and 1-Np^+-N_2,[36] the H-bound isomer corresponds to the most stable Im^+-N_2 structure. The lack of detection of $Im^+-N_2(\pi)$ demonstrates that the π-bound structure is a substantially less stable local minimum. Similarly, π-bound isomers were not observed in the IRPD spectra of An^+-N_2, $Ph(H)^+-N_2$, and 1-Np^+-N_2.[30,34,36,65] In contrast, π-bound In^+-N_2 could be weakly observed, suggesting that π-bonding becomes competitive with H-bonding for $A(H)^+-N_2$ dimers with less acidic $A(H)^+$.[37] This observation confirms that the NH group in Im^+ is slightly more acidic than in In^+ (vide infra). In line with this trend, N_2 complexes of $A(H)^+$ without acidic functional groups, such as $Bz(H)^+$, prefer π-bonds with N_2 over H-bonds.[42,50,70] Similar to the corresponding Ar complexes, the dissociation energies of $A(H)^+-N_2(\pi)$ are relatively insensitive to the detailed structure of $A(H)^+$.[50] For example, $D_0 = 750 \pm 150$ cm^{-1} for $Ph^+-N_2(\pi)$,[31] 700 ± 200 cm^{-1} for $An^+-N_2(\pi)$,[34] ~ 800 cm^{-1} for $BzH^+-N_2(\pi)$,[50] 650 ± 150 cm^{-1} for 1-$Np^+-N_2(\pi)$,[36] and 750 ± 150 cm^{-1} for the carbenium isomers of $PhH^+-N_2(\pi)$.[72] Hence, $D_0(\pi)$ of Im^+-N_2 may also be estimated to be on the order of 600−900 cm^{-1}, in accordance with the UMP2 calculations, $D_e(\pi) = 1056$ cm^{-1}. In contrast to π-bonding, the strength of the H-bonds in $A(H)^+-N_2$ depends sensitively on the acidity of the proton donor group of $A(H)^+$. The UMP2 calculations yield $D_e(H) = 1807$ cm^{-1} for $Im^+-N_2(H)$. Hence, the values of $D_e(\pi)$ and $D_e(H)$ are consistent with the analysis of the photofragmentation data, $2D_0(\pi) + D_0(H) \sim 3300$ cm^{-1}.

The total interaction in ion−ligand complexes with nonpolar ligands is mainly composed of the two-body interaction terms. The interaction in neutral Ar_2 and $(N_2)_2$ is on the order of $D_e \sim 100$ cm^{-1}.[81,82] Consequently, for any angular orientation the optimal Im^+-L interaction is significantly stronger than the L−L attraction. Hence, the Im^+-L_n cluster growth is mainly driven by the Im^+-L dimer potential, because three-body forces are weak. The derived solvation sequence for the most stable Im^+-L_n complexes starts with the formation of a H-bound Im^+-L dimer core, which is then further solvated by $n - 1$ π-bound ligands. A similar cluster growth process was recently deduced for $Ph(H)^+-L_n$, 1-Np^+-L_n, and An^+-L_n with L = Ar and N_2, which also starts with the solvation of the available acidic protons of the $OH_{(2)}$ and NH_2 groups by H-bound ligands, before further π-bound ligands are attached to the aromatic ring.[31,34−36,72,73]

The plots of ν_{NH} of the most stable Im^+-L_n isomers as a function of the cluster size n in Figure 6 mirror the preferred evolution of the solvation (sub)shells. The first H-bound ligand induces a large red shift in ν_{NH} because of the destabilization of the N−H bond upon intermolecular H-bonding. The magnitude of $\Delta\nu_{NH}$ is correlated with the strength of the intermolecular interaction, leading to a larger shift for $L = N_2$ than for L = Ar. The H-bound Im^+-N_2 dimer is further solvated by π-bound ligands, which induce small incremental blue shifts of ν_{NH}. Thus, π-bound ligands slightly destabilize the intermolecular H-bond to the first ligand via noncooperative three-body forces, which in turn stabilize the intramolecular N−H bond. Because of noncooperative three-body interactions, the magnitude of the incremental blue shift decreases with the number of π-bound ligands in the complex.[29] The ν_{NH} frequencies are not converged at the largest cluster size investigated, because the first solvent shell around Im^+ is not complete at $n = 3$.

Unfortunately, neither Ar nor N_2 matrix isolation studies are available for Im^+,[83] preventing a quantitative comparison of the Im^+-L_n cluster band shifts with the bulk limit ($n \rightarrow \infty$) at the present stage.

Previous spectroscopic studies have shown that the complexation-induced red shift in the proton donor stretch vibration of H-bound XH^+-L dimers, $\Delta\nu_{XH}$, is correlated with the difference in the proton affinities (PAs) of the two bases X and L.[28,31,63,84,85] For a given L, $\Delta\nu_{XH}$ is directly correlated to PA(X): the larger the PA(X), the stronger the intermolecular H−L bond and the larger the $\Delta\nu_{XH}$. This trend can be used to derive unknown PA values of bases X from IR spectra of their XH^+-L dimers. Recently, this procedure was applied to $XH^+ = In^+$ and 1-Np^+ to obtain the first experimental estimates for the PA of the indolyl and 1-naphthoxy radicals.[36,37] The measured relative red shifts $|\Delta\nu_{XH}|/\nu_{XH}$ for a series of XH^+-N_2(H) dimers with XH^+ = $SiOH^+$, Ph^+, *trans*-1-Np^+, In^+, and An^+ decrease as 14.1% > 4.8% > 3.13% > 2.2% > 0.57%, in line with the corresponding increase in PA(X) along this series: 778 < 873 < 908 < 923 < 950 kJ mol^{-1}.[36] The $|\Delta\nu_{NH}|/\nu_{NH}$ ratio for Im^+-N_2(H) of 3.9% determined in the present work is significantly larger than that of In^+-N_2(H), implying that the NH group in Im^+ is considerably more acidic than that in In^+. This trend is also seen in the smaller ν_{NH} frequency of Im^+ compared to that of In^+ (3430 and 3454 cm^{-1}). Linear extrapolation using the data (PA and shifts) of the aromatic cluster ions listed above yields PA ~ 890 kJ mol^{-1} for imidazyl radical.

Similar to ν_{NH}, the ν_{CH} frequencies are a measure of the strength and acidity of the C−H bonds. The calculations demonstrate that all three CH groups in Im^+ feature similar bond lengths and stretch frequencies, implying that they are of comparable acidity. Comparison of the experimental ν_{CH} values of Im (3135−3160 cm^{-1})[59] and Im^+ (~3128 cm^{-1}) confirms the theoretical prediction of a slight decrease in the C−H bond strength upon ionization. The fact that ν_{CH} appears to slightly increase upon sequential N_2 complexation (Table 2) suggests that the C−H bond strength increases again by π-bound solvation. Comparison of ν_{CH} of Im^+ (~3128 cm^{-1}) with those of aromatic C−H stretch modes (sp^2 hybridization of C) of related aromatic molecules illustrates the dependence of the C−H bond strengths upon variation of the details of the molecular structure and composition. For example, the average ν_{CH} value of the smallest aromatic hydrocarbon ion, c-$C_3H_3^+$ (3144 cm^{-1}),[62,86] is slightly larger than that of Im^+. On the other hand, the measured ν_{CH} values of Bz^+ (3093 ± 15 cm^{-1})[42] are somewhat smaller. Interestingly, ν_{CH} of protonated substituted benzene derivatives, such as BzH^+ (3080 and 3110 cm^{-1})[50,70] and the carbenium isomers of PhH^+ (3046 and 3069 cm^{-1}),[65] are significantly smaller. Then again, protonation of the heterocyclic Im molecule (ν_{CH} ~ 3170 cm^{-1} for ImH^+)[43] substantially enhances the C−H bond strength. Interestingly, the ν_{CH} values observed for the related heterocyclic In^+ ion (3071 and 3100 cm^{-1})[69] indicate that at least some of the C−H bonds in In^+ are somewhat more acidic than those in Im^+.

VI. Concluding Remarks

The stepwise microsolvation of the Im^+ cation in the nonpolar solvents argon and molecular nitrogen has been investigated by IR photodissociation spectroscopy and quantum chemical calculations of size-selected Im^+-L_n complexes (L = Ar, N_2). Analysis of the *n*- and L-dependent complexation-induced frequency shifts of the N−H stretch vibrations demonstrates that the preferred ion−ligand binding motif between Im^+ and L is H-bonding to the acidic NH group, whereas π-bonding to the aromatic ring and H-bonding to the CH groups are less favorable. Consequently, the preferred Im^+-L_n cluster growth begins with the formation of H-bound Im^+-L dimers, which are further solvated by $n - 1$ π-bound ligands. The $\Delta\nu_{NH}$ shift of Im^+-N_2(H) yields a first experimental estimate for the proton affinity of the imidazyl radical of ~890 ± 30 kJ mol^{-1}, demonstrating that IR spectroscopy of cluster ions can be used to probe thermochemical properties of transient radicals. The most stable Im^+-Ar structure (H-bound isomer) differs qualitatively from that of the neutral dimer (π-bound isomer), emphasizing the large impact of ionization on the interaction potential and the preferred recognition motif between acidic aromatic molecules (A) and nonpolar ligands. The ionization-induced $\pi \rightarrow$ H switch in the preferred binding type in $A^{(+)}-Ar$ complexes has now been established for a large variety of $A^{(+)}$ molecules with acidic functional YH_k groups (Y = O, N) and seems to be a general phenomenon.[29] Significantly, the IRPD spectra of Im^+-L_n yield the first spectroscopic information about the ν_{CH} and ν_{NH} vibrations of bare Im^+, demonstrating that IR spectroscopy of cluster ions can also be used to probe fundamental properties of isolated ions (messenger technique). Comparison between ν_{CH} and ν_{NH} of Im and Im^+ suggests that ionization enhances the acidity of both the C−H and N−H bonds of this fundamental biomolecular building block.

Acknowledgment. This study was supported by the *Deutsche Forschungsgemeinschaft* (Grant DO 729/2-2) and the *Fonds der Chemischen Industrie*. O.D. is supported by a Heisenberg Fellowship (Grant DO 729/1-2).

References and Notes

(1) Stryer, L. *Biochemistry*; Freeman: New York, 1996.
(2) Noguchi, T.; Inoue, Y.; Tang, X. *Biochemistry* **1999**, *38*, 399.
(3) Kyte, J. *Mechanisms in Protein Chemistry*; Garland: New York, 1995.
(4) Bachovchin, W. W. *Biochemistry* **1986**, *25*, 7751.
(5) Brutschy, B. *Chem. Rev.* **1992**, *92*, 1567.
(6) Brutschy, B. *Chem. Rev.* **2000**, *100*, 3891.
(7) Kim, K. S.; Tarakeshwar, P.; Lee, J. Y. *Chem. Rev.* **2000**, *100*, 4145.
(8) Meyer, E. A.; Castellano, R. K.; Diederich, F. *Angew. Chem., Int. Ed.* **2003**, *42*, 1210.
(9) Serrano-Andres, L.; Fülscher, M. P.; Roos, B. O.; Merchan, M. *J. Phys. Chem.* **1996**, *100*, 6484.
(10) Müller-Dethlefs, K.; Dopfer, O.; Wright, T. G. *Chem. Rev.* **1994**, *94*, 1845.
(11) Kleinermanns, K.; Gerhards, M.; Schmitt, M. *Ber. Bunsen-Ges. Phys. Chem.* **1997**, *101*, 1785.
(12) Neusser, H. J.; Krause, H. *Chem. Rev.* **1994**, *94*, 1829.
(13) Caminati, W.; Melandri, S.; Millemaggi, A.; Favero, P. G. *Chem. Phys. Lett.* **1998**, *294*, 377.
(14) According to extensive literature searches using SciFinder and ISI Web of Science in October 2004.
(15) Schäfer, M.; Pratt, D. W. *J. Chem. Phys.* **2001**, *115*, 11147.
(16) Zierhut, M.; Roth, W.; Dümmler, S.; Fischer, I. *Chem. Phys.* **2004**, *305*, 123.
(17) Fujii, A.; Miyazaki, M.; Ebata, T.; Mikami, N. *J. Chem. Phys.* **1999**, *110*, 11125.
(18) Schmitt, M.; Ratzer, C.; Meerts, L. *J. Chem. Phys.* **2004**, *120*, 2752.
(19) Van Bael, M.; Smets, J.; Schoone, K.; Houben, L.; McCarthy, W.; Adamowicz, L.; Nowak, M. J.; Maes, G. *J. Phys. Chem. A* **1997**, *101*, 2397.
(20) Carles, S.; Lecomte, F.; Scherman, J. P.; Desfrancois, C. *J. Phys. Chem. A* **2000**, *104*, 10662.
(21) Talbot, F. O.; Simons, J. P. *Eur. Phys. J. D* **2002**, *20*, 389.
(22) Scheiner, S.; Kar, T.; Pattanayak, J. *J. Am. Chem. Soc.* **2002**, *124*, 13257.
(23) Main-Bobo, J.; Olesik, S.; Gase, W.; Baer, T.; Mommers, A. A.; Holmes, J. L. *J. Am. Chem. Soc.* **1986**, *108*, 677.
(24) Cradock, S.; Findlay, R. H.; Palmer, M. H. *Tetrahedron* **1973**, *29*, 2173.
(25) Ramsey, B. G. *J. Org. Chem.* **1979**, *44*, 2093.
(26) Yan, S.; Bu, Y.; Cao, Z.; Li, P. *J. Phys. Chem. A* **2004**, *108*, 7038.

(27) Lias, S. G.; Liebman, J. F.; Levin, R. D. *J. Phys. Chem. Ref. Data* **1984**, *13*, 695.
(28) Bieske, E. J.; Dopfer, O. *Chem. Rev.* **2000**, *100*, 3963.
(29) Dopfer, O. *Z. Phys. Chem.* **2005**, *219*, 125.
(30) Solcà, N.; Dopfer, O. *Chem. Phys. Lett.* **2000**, *325*, 354.
(31) Solcà, N.; Dopfer, O. *J. Phys. Chem. A* **2001**, *105*, 5637.
(32) Solcà, N.; Dopfer, O. *J. Mol. Struct.* **2001**, *563/564*, 241.
(33) Solcà, N.; Dopfer, O. *Chem. Phys. Lett.* **2003**, *369*, 68.
(34) Solcà, N.; Dopfer, O. *J. Phys. Chem. A* **2002**, *106*, 7261.
(35) Solcà, N.; Dopfer, O. *Eur. Phys. J. D* **2002**, *20*, 469.
(36) Andrei, H. S.; Solcà, N.; Dopfer, O. *Phys. Chem. Chem. Phys.* **2004**, *6*, 3801.
(37) Solcà, N.; Dopfer, O. *Phys. Chem. Chem. Phys.* **2004**, *6*, 2732.
(38) Neusser, H. J.; Siglow, K. *Chem. Rev.* **2000**, *100*, 3921.
(39) Bakker, J. M.; Satink, R. G.; von Helden, G.; Meijer, G. *Phys. Chem. Chem. Phys.* **2002**, *4*, 24.
(40) Weber, T.; Smith, A. M.; Riedle, E.; Neusser, H. J.; Schlag, E. W. *Chem. Phys. Lett.* **1990**, *175*, 79.
(41) Fujii, A.; Fujimaki, E.; Ebata, T.; Mikami, N. *J. Chem. Phys.* **2000**, *112*, 6275.
(42) Dopfer, O.; Olkhov, R. V.; Maier, J. P. *J. Chem. Phys.* **1999**, *111*, 10754.
(43) Andrei, H. S.; Solcà, N.; Dopfer, O. Unpublished results, 2004.
(44) Dopfer, O. *Int. Rev. Phys. Chem.* **2003**, *22*, 437.
(45) Dopfer, O.; Roth, D.; Maier, J. P. *Int. J. Mass Spectrom.* **2002**, *218*, 281.
(46) Olkhov, R. V.; Nizkorodov, S. A.; Dopfer, O. *Chem. Phys.* **1998**, *239*, 393.
(47) Linstrom, P. J.; Mallard, W. G. *NIST Chemistry WebBook*; NIST Standards and Technology: Gaithersburg, MD, 2001 (http://webbook.nist.gov).
(48) Solcà, N.; Dopfer, O. *Chem. Phys. Lett.* **2001**, *347*, 59.
(49) Solcà, N.; Dopfer, O. *J. Am. Chem. Soc.* **2003**, *125*, 1421.
(50) Solcà, N.; Dopfer, O. *Chem.—Eur. J.* **2003**, *9*, 3154.
(51) Olkhov, R. V.; Nizkorodov, S. A.; Dopfer, O. *J. Chem. Phys.* **1998**, *108*, 10046.
(52) Dopfer, O.; Olkhov, R. V.; Maier, J. P. *J. Phys. Chem. A* **1999**, *103*, 2982.
(53) Dopfer, O.; Roth, D.; Maier, J. P. *J. Phys. Chem. A* **2000**, *104*, 11702.
(54) Dopfer, O.; Solcà, N.; Olkhov, R. V.; Maier, J. P. *Chem. Phys.* **2002**, *283*, 85.
(55) Guelachvili, G.; Rao, K. N. *Handbook of Infrared Standards*; Academic Press: London, 1993.
(56) Camy-Peyret, C.; Flaud, J. M.; Guelachvili, G.; Amiot, C. *Mol. Phys.* **1973**, *26*, 825.
(57) Frisch, M. J.; et al. *Gaussian 03*, Revision B.01., Gaussian, Inc.: Pittsburgh, PA, 2003.
(58) Boys, S. F.; Bernardi, F. *Mol. Phys.* **1970**, *19*, 553.
(59) King, S. T. *J. Phys. Chem.* **1970**, *74*, 2133.
(60) Cioslowski, J.; Hay, P. J.; Ritchie, J. P. *J. Phys. Chem.* **1990**, *94*, 148.
(61) Olkhov, R. V.; Nizkorodov, S. A.; Dopfer, O. *J. Chem. Phys.* **1997**, *107*, 8229.
(62) Roth, D.; Dopfer, O. *Phys. Chem. Chem. Phys.* **2002**, *4*, 4855.
(63) Olkhov, R. V.; Dopfer, O. *Chem. Phys. Lett.* **1999**, *314*, 215.
(64) Dopfer, O.; Roth, D.; Maier, J. P. *J. Am. Chem. Soc.* **2002**, *124*, 494.
(65) Solcà, N.; Dopfer, O. *J. Am. Chem. Soc.* **2004**, *126*, 1716.
(66) Hirschfelder, J. O.; Curtis, C. F.; Bird, R. B. *Molecular Theory of Gases and Liquids*; Wiley: New York, 1954.
(67) Gray, C. G.; Gubbins, K. E. *Theory of molecular fluids*; Clarendon: Oxford, 1984.
(68) Buckingham, A. D. *Adv. Chem. Phys.* **1967**, *12*, 107.
(69) Unterberg, C.; Jansen, A.; Gerhards, M. *J. Chem. Phys.* **2000**, *113*, 7945.
(70) Solcà, N.; Dopfer, O. *Angew. Chem., Int. Ed.* **2002**, *41*, 3628.
(71) Siglow, K.; Neuhauser, R.; Neusser, H. J. *J. Chem. Phys.* **1999**, *110*, 5589.
(72) Solcà, N.; Dopfer, O. *J. Chem. Phys.* **2004**, *120*, 10470.
(73) Solcà, N.; Dopfer, O. *Chem. Phys. Lett.* **2001**, *342*, 191.
(74) Dopfer, O.; Engel, V. *J. Chem. Phys.* **2004**, *121*, 12345.
(75) Nizkorodov, S. A.; Dopfer, O.; Ruchti, T.; Meuwly, M.; Maier, J. P.; Bieske, E. J. *J. Phys. Chem.* **1995**, *99*, 17118.
(76) Dopfer, O.; Nizkorodov, S. A.; Olkhov, R. V.; Maier, J. P.; Harada, K. *J. Phys. Chem. A* **1998**, *102*, 10017.
(77) Gascooke, J. R.; Lawrance, W. D. *J. Phys. Chem. A* **2000**, *104*, 10328.
(78) Bellm, S. M.; Moulds, R. J.; Lawrance, W. D. *J. Chem. Phys.* **2001**, *115*, 10709.
(79) Braun, J. E.; Mehnert, T.; Neusser, H. J. *Int. J. Mass Spectrom.* **2000**, *203*, 1.
(80) Dessent, C. E. H.; Haines, S. R.; Müller-Dethlefs, K. *Chem. Phys. Lett.* **1999**, *315*, 103.
(81) Hutson, J. M. *Annu. Rev. Phys. Chem.* **1990**, *41*, 123.
(82) Aquilanti, V.; Bartolomei, M.; Cappelletti, D.; Carmona-Novillo, E.; Pirani, F. *J. Chem. Phys.* **2002**, *117*, 615.
(83) Jacox, M. E. *J. Phys. Chem. Ref. Data* **1998**, *27*, 115.
(84) Fujii, A.; Ebata, T.; Mikami, N. *J. Phys. Chem. A* **2002**, *106*, 8554.
(85) Jacox, M. E. *Chem. Soc. Rev.* **2002**, *31*, 108.
(86) Craig, N. C.; Pranata, J.; Reinganum, S. J.; Sprague, J. R.; Stevens, P. S. *J. Am. Chem. Soc.* **1986**, *108*, 4378.